Geosci. Instrum. Method. Data Syst. Discuss., https://doi.org/10.5194/gi-2018-2
Manuscript under review for journal Geosci. Instrum. Method. Data Syst.
Discussion started: 11 April 2018

Geoscientific Instrumentation Methods and Data Systems
Open Access
Discussions

Laboratory Spectral Calibration of the TanSat Atmospheric Carbon Dioxide Grating Spectrometer

Zhongdong Yang[1], Yuquan Zhen[2], Zenshan Yin[3], Chao Lin[2], Yanmeng Bi[1], Wu Liu[3], Qian Wang[1], Long Wang[2], Songyan Gu[1], and Longfei Tian[3]

[1]National Satellite Meteorological Centre (NSMC), CMA, CHINA
[2]Changchun Institute of Optics Fine Mechanics and Physics (CIOFMP), CAS, CHINA
[3]Shanghai Engineering Centre for Microsatellites (SECM), CAS, CHINA

Correspondence to: Zhongdong Yang (emails: zhongdong.yang@icloud.com, and yangzd@cma.cn)

Abstract. TanSat is a key satellite mission in the Chinese Earth Observation program and is designed to measure the global atmospheric column-averaged dry-air CO_2 mole fraction by measuring the visible and near-infrared solar-reflected spectra. The first Chinese super-high-resolution grating spectrometer for measuring atmospheric CO_2 is aboard TanSat. This spectrometer is a suite incorporating three grating spectrometers that make coincident measurements of reflected sunlight in the near-infrared CO_2 band near 1.61 and 2.06 micrometers and in the molecular oxygen (O_2) A band at 0.76 micrometers. Their spectral resolving power ($\lambda/\Delta\lambda$) are $\sim$19000, $\sim$12800 and $\sim$12250 in O_2 A-band, WCO_2 and SCO_2 band respectively. This paper describes the prelaunch spectral calibration of the Atmospheric Carbon dioxide Grating Spectrometer aboard TanSat. Several critical aspects of the spectrometer, including the spectral resolution, spectral dispersion and the instrument line shape function of each channel, that are directly related to producing the Level 1 products were evaluated in this paper. The instrument line shape function of the spectrometer is notably symmetric and perfectly consistent across all channels in three bands. The variations resulting in spectral calibrations and radiometric response errors are negligible. The spectral resolution characterizations meet the mission requirements. The spectral dispersions have excellent consistency in the spatial dimension of each band, and there is good linearity in the spectral dimension of each band. Taken together, these results suggest that the spectral characterizations of the spectrometer aboard TanSat meet the mission requirements.

1 Introduction

Space-based measurements of atmospheric carbon dioxide using the reflected near-infrared spectrum have the advantage of providing a high sampling sensitivity near the surface of the Earth (Kuang et al., 2002)(Crisp et al., 2004). The Japanese Greenhouse Gases Observing Satellite (GOSAT) and the Orbiting Carbon Observatory-2 (OCO-2) of NASA have been in orbit since 2009 and 2014, respectively(Sakuma and Fumihiro Bruegge, 2010)(Pollock et al., 2010)(Crisp et al., 2017). TanSat is a mission that is designed to measure the global column-averaged atmospheric carbon dioxide and was funded by the Chinese Earth Observation Program, Ministry of Science and Technology (MOST). TanSat was launched successfully into a 705-km sun-synchronous orbit on Dec. 22, 2016. TanSat carries primarily instrumentation, including the Atmospheric Carbon dioxide Grating Spectrometer (ACGS), which has a wide dynamical range and a high spectral resolution. The ACGS incorporates three co-boresighted, long-slit imaging grating spectrometers to measure reflected solar radiation in the oxygen O_2 A band spectrum, which is centered at 760 nm, and in the weak and strong CO_2 bands at 1610 nm and 2060 nm, respectively.

This work presents the prelaunch spectral calibration of the ACGS, which was carried out during thermal vacuum testing of the instrument in Feb. 2016. Several critical aspects, including the instrument spectral resolution, instrument line shape (ILS) and spectral dispersion, were carefully characterized during this testing. All of these aspects are directly related to the quality of the Level 1 products. In our work, we use the full width at half maximum (FWHM) of the ILS to represent the spectral resolution. The ILS, also called the spectral response function, characterizes the relative response of each detector element at the focal plane array of the instrument to monochromatic illumination within the desired spectral range. Dispersion represents the function that specifies the central wavelengths of each detector element. The preflight spectral calibrations of the Orbiting Carbon Observatory (OCO) and OCO-2 were described in detailed by Jason O. Day et al. and Richard A.M. Lee et al., respectively(Day and O'Dell., 2011)(Lee and etc., 2017). C. Frankenberg et al. evaluated the spectrometer performance of OCO-2 using prelaunch direct sun measurements(Frankenberg et al., 2015). The ACGS spectral calibration method is a modified version adapted from that used for OCO and OCO-2 because both instruments shared a similar framework of optical design to that aboard TanSat and use diffraction grating and a two-dimensional focal plane array to collect solar light. There are also have some differences in details between OCO-2 and TanSat. For example, diffuse reflectance method be used on-orbit calibration in TanSat, but OCO-2 uses diffuse transmission method. We also improved the coverage scale of the scanned spectrum in the ACGS spectral calibration. For example, the response of each pixel of the ACGS was directly and automatically scanned by a tunable diode laser without any gaps in the range of each band except for 7 nm at longer wavelengths in the SCO_2 band that were extrapolated based on another 33-nm range measured in the SCO_2 band.

This paper is organized as follows. Section two gives a description of the spectral requirements for the instrument. Section three presents the prelaunch spectral calibration methodology, including the testing equipment, and the data processing method. Section four provides the spectral calibration results. The final section summarizes this work and presents a review of the spectral characterization of this instrument.

2 Overview of ACGS

The ACGS consists of three spectrometers targeting the O_2 A, WCO_2, and SCO_2 bands. These spectrometers are integrated into a common structure to improve system rigidity and thermal stability. A telescope system with a focal length of 252 mm and an IFOV of $0.0818° \times 0.00456°$ is shared by the three spectrometers through a series of beam splitters and re-imagers. The O_2 A band spectrometer produces an image on a 1242×320-pixel focal plane array, and each CO_2 band spectrometer produces an image on a 500×256-pixel focal plane array. Each 140 mm $\times$ 190-mm diffractive grating is a pivotal component for the three spectrometers. The diffractive efficiency of each grating is above 80%, and the wavefront is one-fourth of the wavelength. At the focus of the diffractive grating of each spectral band, a two-dimensional detector collects the radiance. One dimension is used to detect the field of view along the slit as the spatial dimension, and the other dimension measures different wavelengths as the spectral dimension. The detector for the O_2 A band comprises 1242 (spectral dimension) $\times$ 320 (spatial

Geosci. Instrum. Method. Data Syst. Discuss., https://doi.org/10.5194/gi-2018-2
Manuscript under review for journal Geosci. Instrum. Method. Data Syst.
Discussion started: 11 April 2018

dimension) arrays, while the other two detectors for CO_2 comprise 500 (spectral dimension) × 256 (spatial dimension) arrays. In the spectral dimension, in order to have a spectral sampling of more than two detector elements per FWHM in the range of each CO_2 band, the spectral resolution in the two CO_2 bands is slightly lower than that of OCO-2. In the spatial dimension, sets of 24 channels were combined to yield 9 useful spatial footprints so that each footprint would have had a ∼2-km size on the ground.

2.1 Spectral Performance Requirements

As illustrated by Kuang et al(Kuang et al., 2002) and D. Crisp et al(Crisp et al., 2004), three bands in the visual and near-infrared solar-reflected spectra are required to accurately measure atmospheric CO_2 and to efficiently eliminate the impacts of aerosols and clouds (Cressie et al., 2016). Table 1 shows a summary of the ACGS spectral requirements, including the spectral ranges and resolutions. The spectral regions shown in Table 1 are selected because these regions are relatively free of absorption by other gases. High-spectral resolutions can yield greater sensitivity while providing a low signal-to-noise ratio (SNR). In order to have a high SNR and a spectral sampling of more than two detector elements per FWHM, the spectral resolutions in the two CO_2 bands are slightly lower compared to that of the OCO-2.

Table 1. Summary of ACGS Spectral Requirements

	O_2 A	WCO_2	SCO_2
Spectral Range (nm)	758 - 778	1594 - 1624	2042 - 2082
Spectral Resolution (nm)	0.033 - 0.047	0.120 - 0.142	0.160 - 0.182
Signal-to-Noise Ratio	360	250	180
Spectral Sampling Per FWHM	> 2		
IFOV (Km^2)	2×2		
Frame Rate(Hz)	∼3		

2.2 Basic Optical and Electrical Components of the ACGS

The ACGS mainly consists of a pointing mirror, a telescope system, beam splitters, focusing systems, slits, a collimating lens, plane gratings, and focal plane imaging systems. The pointing mirror, which is mounted on a one-dimensional rotation mechanism, is a specially designed optical element with two sides: the front side was designed and processed to be a mirror for reflecting the earthshine spectrum to the telescope, and the back side was designed and prepared by physical grinding and chemical etching to be a 90% reflecting diffuser for on-board solar calibration.

The optical design of the telescope system was based on a coaxial double parabolic crossed planar optical system with a beam contraction ratio of 3:2. A linear polarizer was placed in front of the slit of each spectrometer. The reflected light from the fore-optics system reaches the entrance slits of three spectrometers after being split, converged and polarized by the beam splitters, condenser lenses and polarizers, respectively. In each spectrometer, the light from the slit is collimated and directed to the plane grating. The image of the slit is formed on the focal plane array after diffracted light passes through the optical imaging system.

The spectral range in which the three spectrometers, which use three specifically designed holographic plane gratings in different bands, are arranged is as follows: the O_2 A band (758 -778 nm), the weak CO_2 band (1594 -1624 nm) and the strong CO_2 band (2041 - 2081 nm). A folding mirror is used instead of the beam splitter for the last strong CO_2 band. The spectral dispersion of each spectrometer is determined mainly by the holographic plane grating used for each measured spectral band. In order to reduce the effect of stray light, a narrow-band isolation filter is placed between the beam splitter and condenser lens for the O_2 A band, and the filters are placed in front of the detectors for the weak and strong CO_2 bands in the ACGS. To compensate for aberration, to correct the smile effect and to square the slit image on the focal plane, a slightly curved entrance slit was used for each spectrometer. Since an increase in the area of the detector can effectively improve the SNR for an optical system with a fixed relative aperture, the detector-merging method is employed in the ACGS. In the spatial dimension, a certain number of detectors are combined into one to meet the ground resolution requirement of $2Km \times 2Km$.

3 Methodology

For high-spectral resolution spectrometers, there are many spectral calibration methods that are based on the use of quasi-monochromatic stimuli spectral light sources, gas absorption cells, atomic emission lines, tunable lasers, and solar spectra (Gaiser et al., 2003)(Day and O'Dell., 2011). The tunable laser method has the advantage of high precision. We established the configuration including a tunable diode-laser and wavemeter in our spectral calibration of TanSat. The tunable laser method requires waiting for frequency and intensity stabilization and is thus time consuming. In order to improve the efficiency of the spectral calibration, we devised an automatic measurement device that can continuously measure and scan the spectrum continuously without manual intervention.

3.1 Laboratory Testing Equipment

Determining the ILS for each spectral channel, footprint and band was the central challenge in the ACGS spectral calibration. In the ACGS, there are 20178 individual ILS functions in the three bands in total. For OCO and OCO-2, only portions of the ILS functions were directly scanned(Day and O'Dell., 2011; Lee and etc., 2017), while the other ILS functions were calculated by polynomial ILS interpolation across spectral bands in order to reduce the amount of time-consuming work. In our work, except for a very small 7-nm region of the SCO_2 band, all of the ILS profiles of the ACGS were scanned directly by three tunable diode lasers without any gaps in the range of each band. The lasers had very a narrow line width (<300 kHz), and the step size was two orders of magnitude smaller than the FWHM in each band. The stability of the laser at the desired wavelength is better than 5 pm, but tens of seconds were required to stabilize the laser. Table 2 shows the key parameters of the tunable laser. A wavemeter with an accuracy of 0.2 pm, manufactured by the Bristol Instrument Company, was used to monitor the laser wavelength accuracy and stability. Table 3 shows the relevant parameters of the wavemeter. Laser speckle can severely affect the light on the focal plane and then cause random fluctuations in the final ILS functions. Laser speckle was removed using a spinning ground glass disk while reducing the laser intensity by approximately 20%.

Table 2. Summary of the Tunable Diode Laser Parameters

Type	TLB6172	TLB6730	TLB6736
Wavelength Range (nm)	758 - 778	1550 - 1630	1975 - 2075
Minimum power (mW)	5	4	2
Line widths (kHz)	<300	<300	<300
Stability(nm/15 s)	<0.001	<0.001	<0.001

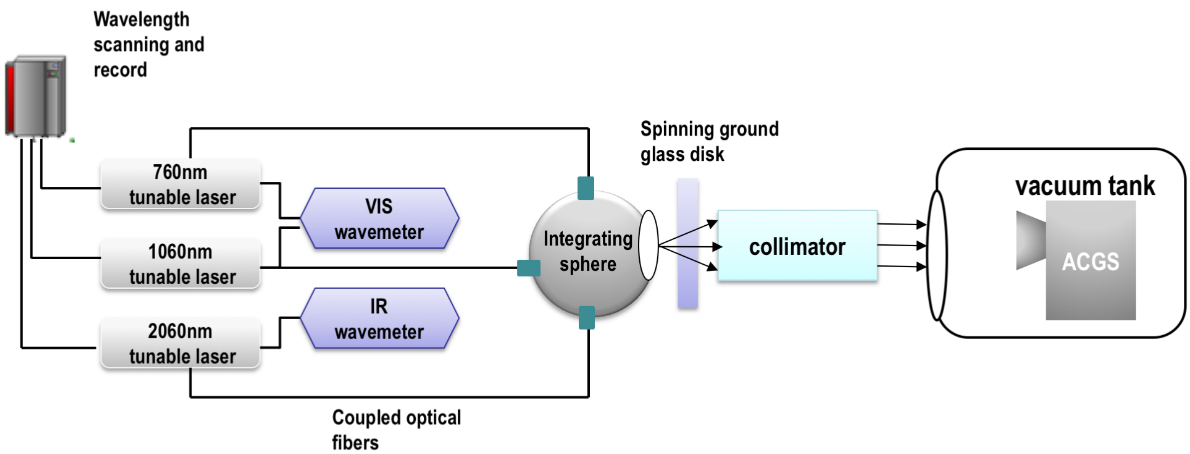

Figure 1. Schematic diagram of the ACGS spectral calibration

Table 3. Summary of the Wavemeter Parameters

Type	621B-NIR.	621B-IR
Range of wavelength (nm)	600 -1800	1500 - 4000
Accuracy of wavelength (ppm)	±0.2	±1
Sampling rate (Hz)	1	1
Input power (μW)	⩾20	⩾1

The laboratory setup and the schematic diagram of the ACGS spectral calibration are presented in Fig. 1. An automatic ILS measurement device was devised in this work. The device consists of a tunable diode laser, which was fiber coupled to both a wavemeter and a 2-inch Labsphere integrating sphere, collimator, and programming control system. This device can scan the spectrum and confirm the stability of the wavelength and intensity automatically according to specified settings. This system improved the measurement efficiency remarkably.

3.2 Data Processing Procedure

The scan range of the tunable diode laser used to determine detailed characterizations of single ILS functions was greater than ±5 FWHMs. By averaging tens of frames, some random noise in the laser and detector can be eliminated. After the whole ranges of each band were scanned, the raw ILS profiles for each channel can be generated. The centroid wavelength response of each channel can be found by the Gaussian fits to the raw ILS profiles. Then, the spectral polynomial fits can be used to calculate the dispersion coefficients. The spectral resolution expressed in FWHMs can also be calculated and assessed. Fig. 2 presents a flowchart of the data processing procedure to determine the ILS, resolution and dispersion coefficients for each channel in each band. Because each channel was scanned by a tunable diode laser, this processing method was used for all channels to analyze the spectral parameters.

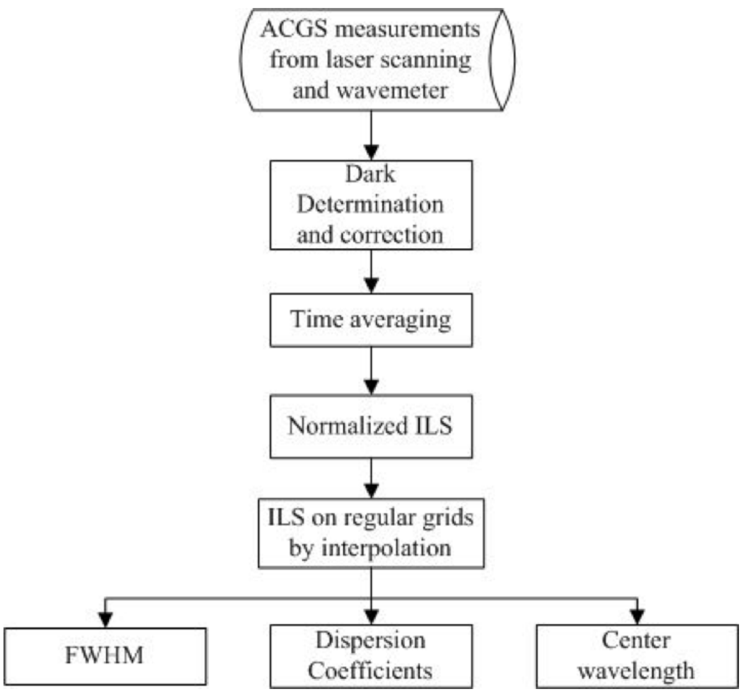

Figure 2. Flowchart of instrument spectral calibration data processing

4 Results

4.1 ILS Profile

The ILS profile, i.e., the spectral response function of each channel, is one of the core parameters of high-spectral resolution instruments. The shape and consistency of the ILS profiles in a band are two key characteristics that indicate the precision of the spectral calibration(Sun et al., 2017; Beirle et al., 2017).

As can be seen in Fig. 3, the ILSs of the first 60 channels of footprint 5 in the O_2 A band, which ranges from 757.42 to 758.50 nm, the first 25 channels in the WCO_2 band, which ranges from 1594.0 to 1595.5 nm, and in the SCO_2 band, which ranges from 2040.54 to 2042.56 nm, are always noticeably symmetric and perfectly consistent across these channels.

In order to evaluate the ILS in depth, we assumed the ILS profile of the center channel, i.e., 621 channel of footprint 5, as a standard for comparison with other footprints in the first, center, and last channels in the three bands. We call the variation of each point the ILS bias. As detailed in Fig. 4, there is very small ILS bias in the spatial and spectral dimensions in the three bands. The ILS bias between the profiles of 621 channel of footprint 5 and other footprints of the O_2 A band was -0.0052 to 0.0071% in channel 1; less than ±0.005% and more symmetric in channel 621; and -0.029 to 0.012% in channel 1242, i.e., the last channel. The ILS biases between footprint 5 and other footprints of the WCO_2 band are -0.0066 to 0.0127% in channel 1; -0.009.8 to 0.0072% in channel 250; and -0.0155 to 0.0074% in channel 500, i.e., the last channel in WCO_2. There is noticeable symmetry in the ILS results for the WCO_2 band band. The ILS biases between footprint 5 and other footprints of the SCO_2 band are -0.0041 to 0.0033% in channel 1; -0.0053 to 0.0029% in channel 250; and -0.0183 to 0.0145% in last channel, which is perfectly consistent with previous results.

4.2 Spectral Dispersion

As seen in Fig. 5, the spectral dispersion coefficients have excellent consistency in the 9 footprints of each band and exhibit very good linearity in the spectral dimension of each band. A fifth-order polynomial fitting method is sufficient to model the tunable diode laser dispersion in each band, and the RMS errors of the fitting residuals are 0.9 pm, 1 pm, and 0.7 pm in theO_2 A band, the WCO_2 band and the SCO_2 band, respectively. These errors are negligible. In fact, only the first three low-order items of the fitted multinomial coefficients are significant; other two high-order items are not significant.

We summed the ILS profile variation in the comparisons above to obtain the area variation in the ILS profile. This measure can be thought of as the spectral response variation between footprint 5 and the other footprints in the spatial dimension. The maximum response variations are 0.5%, 0.09%, and -1.62% in the first, middle and last channels in the O_2 A band; 0.63%, 0.38%, and -0.52% in the first, middle and last channel in the WCO_2 band; and 0.21%, -0.15%, 0.33% in the first, middle and last channel in the WCO_2 band, respectively. On the whole, the consistency of the ILS values across the spatial and spectral dimensions is perfect in the three bands. Most of the ILS response variations are less than 0.63%. The maximum ILS variation was -1.62% in last channel of O_2 A band between footprint 1 and footprint 5. Most of the bias is present at both wings of ILS profiles and is negligible at the centroid wavelength of the ILS. Thus, the ILS variations resulting in changes in radiometric response and spectral dispersion are of little significance.

Geosci. Instrum. Method. Data Syst. Discuss., https://doi.org/10.5194/gi-2018-2
Manuscript under review for journal Geosci. Instrum. Method. Data Syst.
Discussion started: 11 April 2018

Geoscientific Instrumentation Methods and Data Systems
Open Access
Discussions

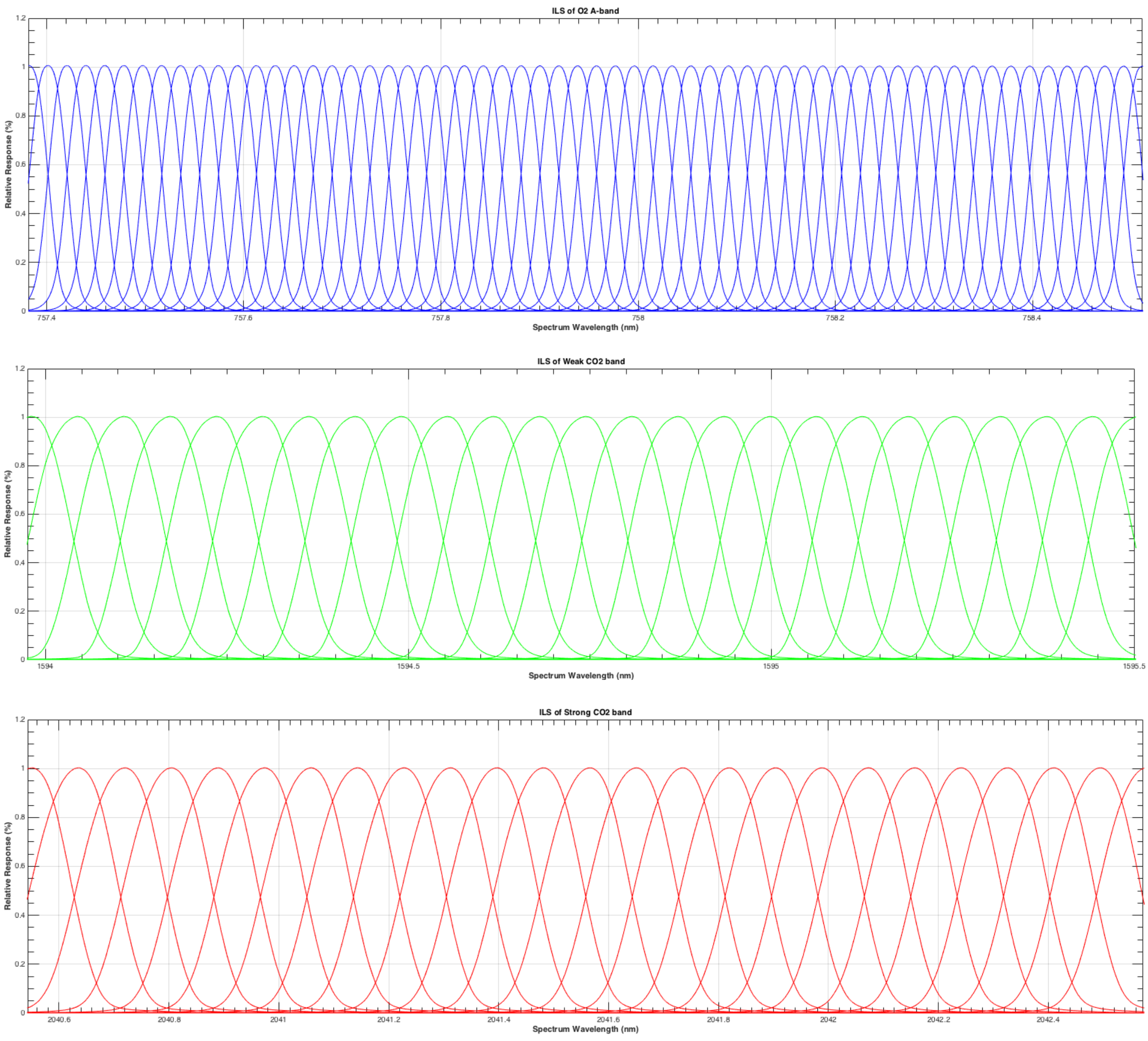

Figure 3. ILS of the first 60 channels in the O_2 A-band (top), first 25 channels in the WCO_2 (middle) band and the SCO_2 (bottom) bands of footprint 5

Geoscientific Instrumentation Methods and Data Systems Discussions

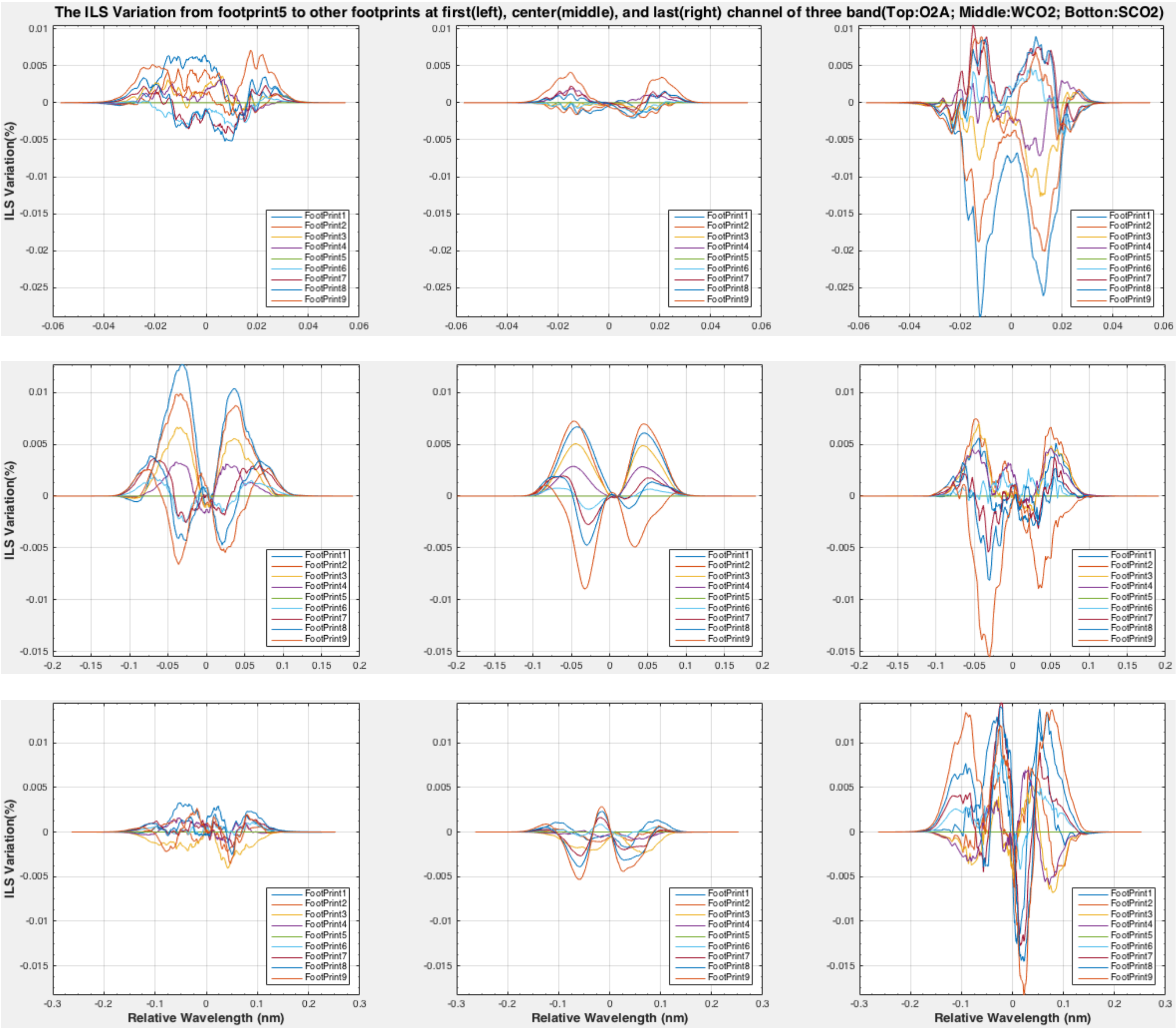

Figure 4. The ILS bias between the center of footprint 5 and the other footprints in the first, center, and last channels in the three bands. The top row is the O_2 A-band, the middle row is the SCO_2 band, and the bottom row is the SCO_2 band. The left column is the first channel in the three bands, the middle column is the center channel, and the right column is the last channel in the three bands. Different colors represent the ILS biases between footprint 5 and different footprints.

Geosci. Instrum. Method. Data Syst. Discuss., https://doi.org/10.5194/gi-2018-2
Manuscript under review for journal Geosci. Instrum. Method. Data Syst.
Discussion started: 11 April 2018

Geoscientific Instrumentation Methods and Data Systems
Discussions

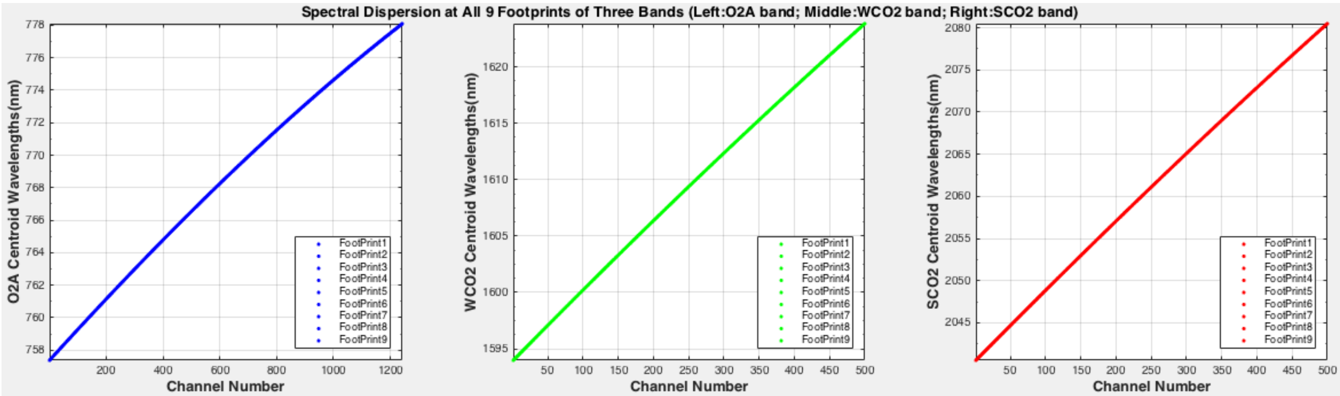

Figure 5. The spectral dispersion at all 9 footprints of the three bands (left:the O_2 A-band; middle: the WCO_2 band; right: the SCO_2 band). Because the spectral dispersion were perfect consistency between these footprints, the points of each footprint nearly overlap each other.

4.3 FWHM

The FWHM can be used to identify the spectral resolution of hyper-spectrometers. The FWHM was calculated from the ILS values for each channel in the three bands. The FWHMs for all channels are between 0.0393 nm $\sim$ 0.0422 nm in the O_2 A band, 0.123 nm $\sim$ 0.128 nm in the WCO_2 band, and 0.16 nm $\sim$ 0.17 nm in the SCO_2 band. Thus, the spectral resolving power ($\lambda/\Delta\lambda$) values are $\sim$19000, $\sim$12800 and $\sim$12250 in the O_2 A band, the WCO_2 band and the SCO_2 band, respectively, which indicates that the spectral resolution meets the mission requirements.

5 Conclusions

The spectral calibration of a super-high-resolution spectrometer is a big challenge because of the rigid precision requirements and the time-consuming nature of the work. In this study, we devised an elaborate automatic spectral calibration measurement device. The response of each channel of the ACGS was directly and automatically measured by a device that combines a tunable diode laser and a wavemeter, and this device, which was designed and implemented during this work, performs measurements without gaps in the spectral range of each band except for the last 7 nm in the longer wavelengths of the SCO_2 band. Values for these 7 nm were extrapolated from laser measurements of the first 33 nm of the SCO_2 band. Based on these data measured by lasers, we calculated and evaluated the ILS, FWHM and spectral dispersion in each channel of the three bands. The ILSs were detailed in previous section and were noticeably symmetric and perfectly consistent across all channels in the three bands. The variation in ILS resulted in negligible errors in the radiometric response and spectral calibrations. The FWHM characterization meets the mission requirements. The spectral dispersion had excellent consistency in the spatial dimension of each band and had good linearity in the spectral dimension of each band. Taken together, these results suggest that the ACGS spectral characterization meets the mission requirements. These characterizations will be evaluated again during the TanSat checkout on orbit, and the data will be validated using other similar space-based measurements.

Acknowledgements. The authors would like to thank all of the CIOFMP employees who worked wisely and tirelessly to gain the ACGS TVAC data. The research described in this paper was carried out at the NSMC, CIOFMP and SECM under three contracts (2011AA12A104, 201112A102, and 201112A101) under a major project of the Ministry of Science and Technology (MOST) of the China Earth Observation program (863).

References

Beirle, S., Lampel, J., Lerot, C., Sihler, H., and Wagner, T.: Parameterizing the instrumental spectral response function and its changes by a Super-Gaussian and its derivatives, Atmos. Meas. Tech., 10, 581 – 598, https://doi.org/10.5194/amt-2016-307, 2017.

Cressie, N., Wang, R., Smyth, M., and Miller, C. E.: Statistical bias and variance for the regularized inverse problem: Application to space-based atmospheric CO2 retrievals, J. Geophys. Res. Atmos., 121, 5526–5537, https://doi.org/10.1002/2015JD024353, 2016.

Crisp, D., Atlas, R. M., Breon, F. M., Brown, L. R., Burrows, J. P., Ciais, P., Connor, B. J., Doney, S. C., Fung, I. Y., Jacob, D. J., Miller, C. E., O'Brien, D., Pawson, S., Randerson, J. T., Rayner, P., Salawitch, R. J., Sander, S. P., Sen, B., Stephens, G. L., Tans, P. P., Toon, G. C., Wennberg, P. O., Wofsy, S. C., Yung, Y. L., Kuang, Z., Chudasama, B., Sprague, G., Weiss, B., Pollock, R., Kenyon, D., and Schroll, S.: The Orbiting Carbon Observatory (OCO) mission, in: Adv. Sp. Res., vol. 34, pp. 700–709, https://doi.org/10.1016/j.asr.2003.08.062, 2004.

Crisp, D., Pollock, H. R., Rosenberg, R., Chapsky, L., Lee, R. A. M., Oyafuso, F. A., Frankenberg, C., O'Dell, C. W., Bruegge, C. J., Doran, G. B., Eldering, A., Fisher, B. M., Fu, D., Gunson, M. R., Mandrake, L., Osterman, G. B., Schwandner, F. M., Sun, K., Taylor, T. E., Wennberg, P. O., and Wunch, D.: The On-Orbit Performance of the Orbiting Carbon Observatory-2 (OCO-2) Instrument and its Radiometrically Calibrated Products, Atmos. Meas. Tech. Discuss., pp. 1–45, https://doi.org/10.5194/amt-2016-281, http://www.atmos-meas-tech-discuss.net/amt-2016-281/, 2017.

Day, J. O. and O'Dell., C. W.: Preflight Spectral Calibration of the Orbiting Carbon Observatory, IEEE Trans. Geosci. Remote Sens., 49, 2438–2447, https://doi.org/10.1109/TGRS.2010.2090887, http://ieeexplore.ieee.org/lpdocs/epic03/wrapper.htm?arnumber=5673019, 2011.

Frankenberg, C., Pollock, R., Lee, R. A. M., Rosenberg, R., Blavier, J. F., Crisp, D., O'dell, C. W., Osterman, G. B., Roehl, C., Wennberg, P. O., and Wunch, D.: The Orbiting Carbon Observatory (OCO-2): Spectrometer performance evaluation using pre-launch direct sun measurements, Atmos. Meas. Tech., 8, 301–313, https://doi.org/10.5194/amt-8-301-2015, 2015.

Gaiser, S. L., Aumann, H. H., Strow, L. L., Hannon, S. E., and Weiler, M.: In-flight spectral calibration of the Atmospheric Infrared Sounder, IEEE Trans. Geosci. Remote Sens., 41, 287–297, https://doi.org/10.1109/TGRS.2003.809708, 2003.

Kuang, Z., Margolis, J., Toon, G., Crisp, D., and Yung, Y.: Spaceborne measurements of atmospheric CO 2 by high-resolution NIR spectrometry of reflected sunlight: An introductory study, Geophys. Res. Lett., 29, 11–1–11–4, https://doi.org/10.1029/2001GL014298, http://doi.wiley.com/10.1029/2001GL014298, 2002.

Lee, R. A. M. and etc., C. W. O.: Preflight Spectral Calibration of the Orbiting Carbon Observatory 2, IEEE Trans. Geosci. Remote Sens., 49, 2793–2801, https://doi.org/10.1109/TGRS.2011.2107745, 2017.

Pollock, R., Haring, R. E., Holden, J. R., Johnson, D. L., Kapitanoff, A., Mohlman, D., Phillips, C., Randall, D., Rechsteiner, D., Rivera, J., and Others: The Orbiting Carbon Observatory Instrument: performance of the OCO instrument and plans for the OCO-2 instrument, Remote Sens., 7826, 78 260W—-78 260W, https://doi.org/10.1117/12.865243, 2010.

Sakuma and Fumihiro Bruegge, e.: OCO / GOSAT Preflight Cross-Calibration Experiment, IEEE Trans. Geosci. Remote Sens., 48, 585–599, 2010.

Sun, K., Liu, X., Nowlan, C., Cai, Z., Chance, K., Frankenberg, C., Lee, R. A. M., Pollock, R., Rosenberg, R., and Crisp, D.: Characterization of the OCO-2 instrument line shape functions using on-orbit solar measurements, Atmos. Meas. Tech.,, 10, 939–953, https://doi.org/10.5194/amt-2016-335, 2017.